

An experimental study on reentrant corner crack reinforcement for pretensioned, prestressed concrete slabs

Manwoo Kim and Thomas H.-K. Kang

- The purpose of this study was to verify the occurrence of reentrant corner cracks in pretensioned, prestressed concrete slabs and to assess the effectiveness of reinforcement in preventing reentrant corner cracking.
- Four specimens were manufactured and tested. The specimens varied in types of embedded reinforcing elements, including no reinforcing elements, two types of three-dimensional printed reinforcing elements, and metal lath reinforcement.
- This study presents experimental evidence and engineering methodology to advance understanding of reentrant corner cracking.

Precast concrete involves manufacturing reinforced concrete components in a plant and then assembling on-site. Precast concrete components are repeatedly produced in the same shape, and it is crucial to properly place reinforcement during casting to prevent cracks, which can cause problems such as water leakage, corrosion of reinforcement, and structural deterioration.

In pretensioned, prestressed concrete components, prestressing is introduced by the bond mechanism between the strand and concrete (**Fig. 1**). The concrete surrounding the embedded strand can be regarded as a confining element, and the bond stress can be determined by multiplying the confining stress of concrete and the friction coefficient at their interface. This confining stress of concrete has the same value as the expansion pressure acting on the concrete, and the expansion pressure generates tensile stress occurring in the form of a ring around the strand,¹ making the concrete around the strand susceptible to cracking.

The structural efficiency of pretensioned, prestressed concrete slabs is enhanced by forming hollow cores inside the cross section or by reducing specific areas of the cross section. However, if section reduction leads to insufficient concrete cover around the strands, cracks may occur and the serviceability of the concrete slab may decrease.²⁻⁴ Therefore, it is necessary to design the cross section of the slab to prevent cracking by considering the stress distribution of the concrete around the embedded strands.

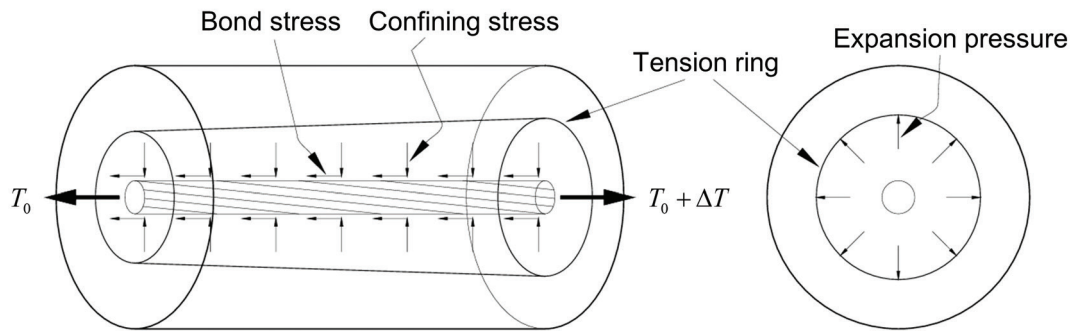


Figure 1. Introduction of prestress by the bond mechanism. Note: T_0 = initial prestress; ΔT = increased prestress due to bond behavior.

A reentrant corner is a point where the internal angle between adjacent surfaces changes abruptly (typically, by about 90 degrees). Localized stress concentration occurs around reentrant corners, increasing the likelihood of diagonal crack formation. In the typical design process, concrete slabs are designed for the ultimate state caused by external loads and crack examination is primarily focused on the top or bottom surfaces.^{5,6} However, in certain cases, such as the dapped end of a precast concrete beam or the reentrant corner of a floor or wall, failure mode due to cracks that are not generally considered in the design process may occur. To prevent reentrant corner cracks, reinforcing bars are placed across the cracks in accordance with design specifications. In this paper, when the cross section of a pretensioned concrete slab has a reentrant corner, diagonal cracks that form around the strand are considered to be a type of reentrant corner. The occurrence of reentrant corner cracks in pretensioned, prestressed concrete slabs has not been clearly confirmed. Nonetheless, as the size of the structure increases, the span becomes longer, requiring higher prestressing on the cross section to resist external forces, which in turn increases the likelihood of cracking.

An inverted ribbed precast concrete slab forms a composite section with cast-in-place concrete placed on the top surface. This type of slab is a cost-effective option in places where the span is not long and the applied load is not large. In addition, this type of slab is suitable for mechanized production, similar to hollow-core slabs. The cross section of an inverted ribbed precast concrete slab consists of a flat lower flange and ribs (Fig. 2). Prestressing is applied at the area where a lower flange and a rib meet, creating a reentrant corner area that receives prestressing. For this reason, experimental verification is necessary to confirm the likelihood of cracks occurring.

Because the strand embedded in concrete by the pretensioning method is attached to the concrete under high tensile stress, it is difficult to identify its behavior by varying the tensile force. Furthermore, in a push-in experiment, the crack pattern in the cross section at the location of maximum stress cannot

be observed. Therefore, a pullout experiment of untensioned strands embedded in concrete was conducted to observe their behavior as the applied tensile force increased. In pullout tests, when tension is applied using a hydraulic jack that blocks the surface, the bond characteristics near the surface are altered due to the arch effect. Moreover, isolating a certain length from the surface to prevent arch effect has the limitation that cracks on the tensile side cannot be observed. This study adopted an alternative experimental method to eliminate the arch effect and enable the observation of the crack patterns on the tensile side.

Reentrant corner cracking of pretensioned, prestressed concrete slabs

In this study, the crack that occurs in a diagonal direction from the strand closest to the reentrant corner (Fig. 2) was called a *reentrant corner crack*. Figure 3 shows actual examples of such cracks. To identify the causes of reentrant corner cracks, it is necessary to consider the manufacturing process

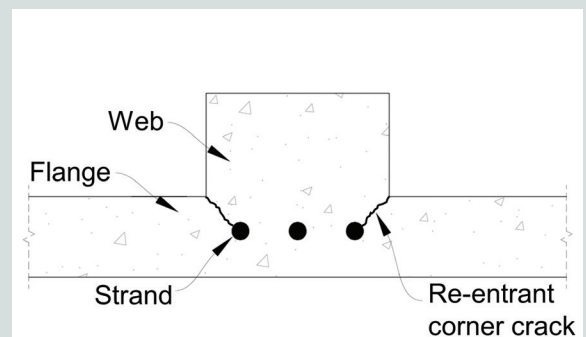


Figure 2. Reentrant corner cracks of a pretensioned concrete slab.



Figure 3. Actual cases of reentrant corner crack formation.

of pretensioned, precast concrete components. The process involves several steps, including mold making, strand tensioning and reinforcement placing, concrete casting, curing, strand cutting, and demolding. Reentrant corner cracks often occur during the strand-cutting process, when the tensile force of the strand is transferred to the concrete as prestressing. These cracks can result from insufficient thickness of the concrete cover around the strand or excessive prestressing introduced to a small area, or they can be due to geometrical stress concentration.

In addition to insufficient concrete cover thickness around the strands and the introduction of excessive prestressing, other factors that can influence the occurrence of reentrant corner cracks are the initial strength of concrete at strand cutting, the impact load effect at strand cutting, and the concentration of stress due to the concave shape of reentrant corners.^{7,8} In this study, all specimens were made of the same concrete mixture and were subjected to gradually increasing loads without impact load effect and with identical chamfer shapes to ensure a uniform stress concentration effect. The experiment was planned to solely compare the behavior based on the magnitude of pullout force.

It is well understood that the drying shrinkage or the applied load of concrete can cause cracking in a diagonal direction around openings in walls and slabs of buildings. To prevent such cracking, reinforcing bars are typically placed at the reentrant corners in a direction perpendicular to the crack surface. The reentrant corner cracks of pretensioned, prestressed concrete slabs exhibit a pattern similar to that of cracks around openings in walls and slabs. Therefore, it is expected that placing reinforcing elements in a perpendicular direction to the anticipated crack surface will effectively prevent cracking. However, for industrial application, it was judged to be inappropriate to place reinforcing bars in precast concrete slabs due to the difficulties in fixing them and the excessive amount of labor required for bar arrangement during the production process. Thus, a novel reinforcing method was used in this investigation.

Literature review

Reentrant corner cracks in pretensioned, prestressed concrete slabs

den Uijl² conducted a study on the development of strand embedded in pretensioning method and observed that reentrant corner cracks often occur in the transfer zone of pretensioned, prestressed concrete components. In that study, the connecting lines of strands and the diagonal connecting line from the outermost strand to the closest concrete cover were defined as a critical path for crack occurrence. That critical path is the same as the reentrant corner crack of the pretensioned, prestressed concrete slab, which is the subject of this study. In addition, the concrete cover thickness to prevent reentrant corner cracking due to the expansion pressure of the strands was presented using the average tensile strength of concrete in den Uijl's study.

Leskelä⁴ noted that shear bond failure can occur due to insufficient anchorage of concrete around strands in a hollow-core slab and used push-out testing to identify the bond characteristics of concrete around strands. Leskelä suggested using the push-out test as a quality control method for precast concrete slabs. The test is similar to the pullout test, but instead of pulling the embedded strand outward, the direction is reversed (toward the inside of the member).

Raja⁹ conducted a finite element analysis on a precast, pretensioned concrete inverted tee beam to identify the area susceptible to cracks. The highest tensile stress occurred at the reentrant corner where the lower flange and the rib meet in the end region, indicating a high possibility of cracking. This result showed that cracking in the reentrant corner is highly likely in pretensioned, precast concrete components.

The behavior of concrete can be expressed by a thick-walled cylinder model, which considers concrete surrounding the embedded strand as a hollow cylinder.^{10,11} In this model, expansion stress resulting from the slip of the strand is exerted

inside the concrete cylinder, leading to cracking if the expansion pressure exceeds the elastic limit. This thick-walled cylinder model implies the possibility that the confinement effect can be increased by reinforcing the crack surface to restrain the crack width. Coccia et al.¹² confirmed that when the concrete around the strand is reinforced with confinement steel, the confinement effect is maintained even as slip increases. In our study, the reinforcing element was designed in an industrially applicable form and was placed on the anticipated crack surface.

Design codes and specifications

The 2010 edition of the *fib* (International Federation for Structural Concrete) *Model Code for Concrete Structures (2010)*¹³ specifies that splitting can occur along the transfer length of a strand embedded by pretension method. The code also specifies that no reinforcement against splitting forces is necessary if the distance between the strands and the cover satisfies the minimum values given in **Table 1**. In this study, the clear cover thickness of the specimens was set to 3ϕ (38.1 mm [1.5 in.]) by referring to the 2010 *fib* model code, where ϕ is the nominal diameter of strand. The 2020 *fib* model code,¹⁴ which was published after the completion of the experiment, specifies smaller clear spacing and cover than the previous version did; therefore, the specimens also comply with the 2020 *fib* model code.

In previous experimental studies,^{15,16} cracks in the concrete around the strands led to the debonding of strands, resulting in a loss of flexure and shear strength. The ninth edition of the American Association of State Highway and Transportation Officials' *AASHTO LRFD Bridge Design Specifications*¹⁷ says that confinement steel must be placed for a distance of $1.5d$ from the end of the bottom flange of the precast concrete beam, where d is the distance from compression face to centroid of tension reinforcement. The confinement reinforcement around the strand is related to the failure mode of the flexural member and so it also must be reviewed for low-height building slabs.

Experimental program

Design of test specimens

The shape of the specimens was derived from the unit rib of an inverted ribbed precast concrete slab commonly used in construction projects. Each specimen had a right-angled edge around the strand where cracks were expected to occur from the outermost strand to the concave part of the reentrant corner during the strand pullout experiment (**Fig. 4**). Each specimen was manufactured by first installing a formwork on the lower structure, which was fabricated to fix the specimen. Strands and reinforcing elements were then placed inside the formwork, followed by concrete placement.

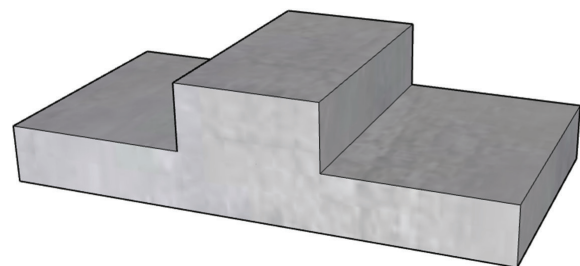
Table 1. Minimum clear spacing and cover in *fib Model Code for Concrete Structures (2010)*

Concrete strength	Minimum clear spacing	Minimum cover
C20/25 to C50/60	3ϕ	3ϕ
	2.5ϕ	4ϕ
$\geq C55/67$	2.5ϕ	2.5ϕ
	2ϕ	3ϕ

Note: ϕ = nominal diameter of strand.



Slab



Test specimen

Figure 4. Ribbed precast concrete slab and test specimen.

The specimens used in the experiment varied in terms of the types of embedded reinforcing elements used to reinforce reentrant corner cracks (**Table 2**). In one of the specimens, the metal lath was arranged so that the long way of the mesh would align with the direction of the strand. One specimen was fabricated and tested for each test configuration.

The PS-NON specimen had no embedded reentrant corner crack reinforcing elements. PS-3DP-HOLLOW and PS-3DP-SOLID specimens had reinforcing elements manufactured by three-dimensional (3-D) printing (**Fig. 5**). Those two specimen types were designed to compare the reinforcing effects associated with the presence (PS-3DP-HOLLOW) or absence (PS-3DP-SOLID) of internal hollows in the reinforcing ele-

ments. Finally, in the PS-MESH specimen, reentrant corners were reinforced using metal lath.

When the strands were pulled out of the specimens, it was expected that the reentrant corner cracks would extend toward the concave part of the corner (**Fig. 2**). Accordingly, the reinforcing elements were embedded perpendicular to the anticipated crack surface.

There was a concern that the 3-D-printed reinforcing elements of PS-3DP-HOLLOW and PS-3DP-SOLID might not adhere well to the concrete. To address this issue, holes were made in the reinforcing elements to which fixing bolts could be connected (**Fig. 5**). Fixing bolts were connected to

Table 2. Summary of test specimens

ID	Embedded strand	Reinforcing method	Fixing method
PS-NON	3 ϕ 12.7	none	none
PS-3DP-HOLLOW	3 ϕ 12.7	3-D printed, hollow	fixing bolt connected and embedded
PS-3DP-SOLID	3 ϕ 12.7	3-D printed, solid	fixing bolt connected and embedded
PS-MESH	3 ϕ 12.7	metal lath	diamond shaped mesh LWM = 30 mm SWM = 15 mm t = 1.2 mm w = 1.8 mm

Note: 3-D = three-dimensional; LWM = long way of mesh; PS-MESH = specimen with reentrant corners reinforced using metal lath; PS-NON = specimen with no reentrant corner crack reinforcing elements; PS-3DP-HOLLOW = specimen with hollow reinforcing elements manufactured by three-dimensional printing; PS-3DP-SOLID = specimen with solid reinforcing elements manufactured by three-dimensional printing; SWM = short way of mesh; t = thickness of strand; w = width of strand; ϕ = nominal diameter of strand. 1 mm = 0.0394 in.

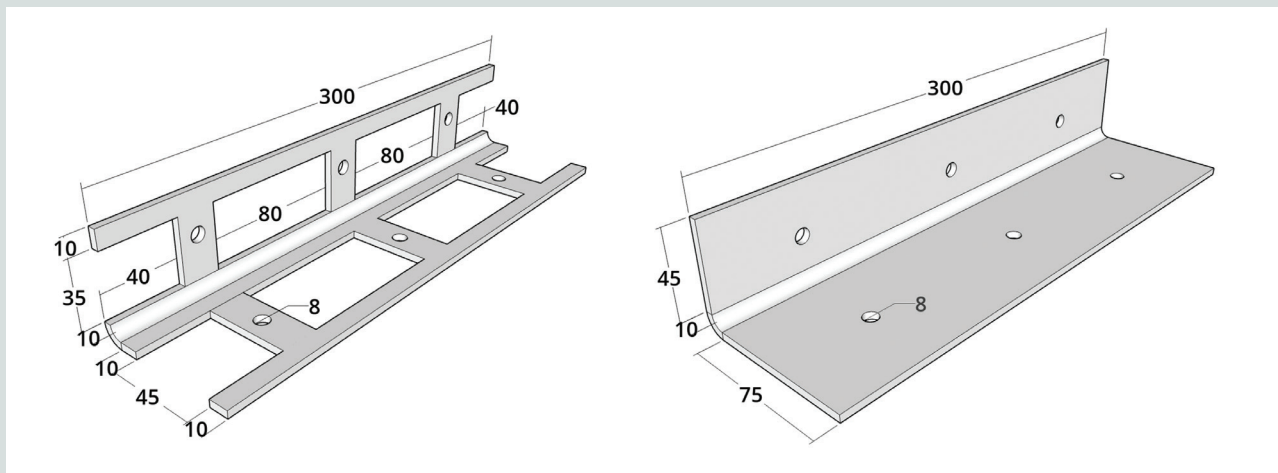


Figure 5. Reinforcing elements for test specimens. Note: All units are in millimeters. PS-3DP-HOLLOW = specimen with hollow reinforcing elements manufactured by three-dimensional printing; PS-3DP-SOLID = specimen with solid reinforcing elements manufactured by three-dimensional printing. 1 mm = 0.0394 in.

the reinforcing elements, and the reinforcing elements were embedded in the concrete. Because the fixing bolts did not cross over the reentrant corner crack surface, it was expected that they would not affect the occurrence of reentrant corner cracking in this experiment.

The four specimens have the same dimensions, as detailed in **Fig. 6**. Untensioned strands were embedded inside the formwork, and the lower structure and the specimen were connected with nine D10 (no. 3) (f_y of 500 MPa [72.5 ksi]) reinforcing

bars. The distance from the outermost strand to the concrete cover was set to 3ϕ (ϕ of the seven-wire strand 12.7 mm [0.5 in.]). Three 12.7 mm diameter strands protruded 470 mm (18.5 in.) from the upper surface of the specimens. **Figure 7** shows the formwork with internal reinforcing elements during the specimen manufacturing process. When the actuator and the strands were connected, the lower surface of the connecting plate and the upper surface of the specimens were separated by 300 mm (11.8 in.) to allow for visual observation of cracks on the upper surface during the pullout experiment.

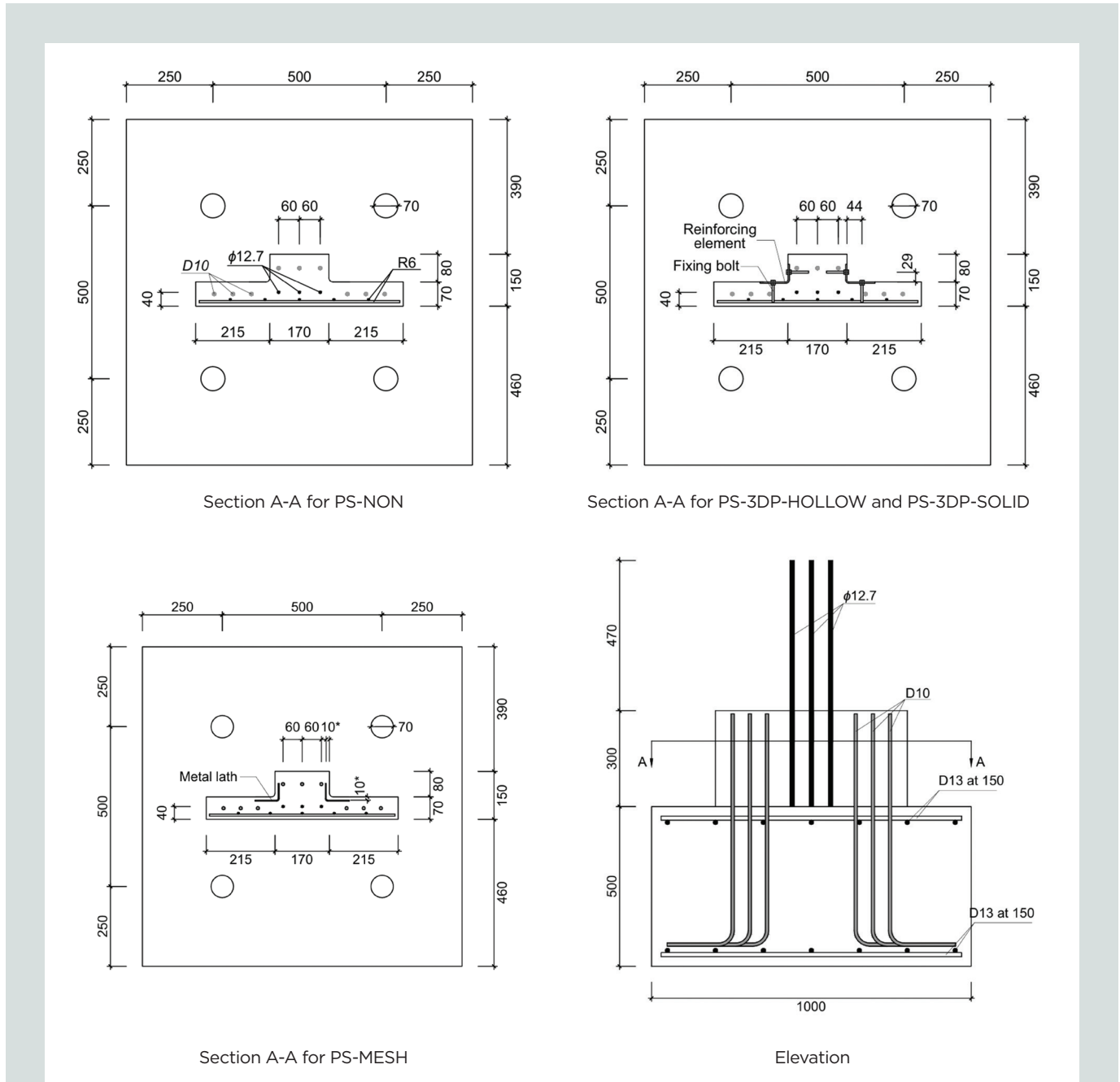


Figure 6. Details of test specimens. Note: All units are in millimeters. D = deformed reinforcing bar; PS-3DP-HOLLOW = specimen with hollow reinforcing elements manufactured by three-dimensional printing; PS-MESH = specimen with reentrant corners reinforced using metal lath; PS-NON = specimen with no reentrant corner crack reinforcing elements; PS-3DP-SOLID = specimen with solid reinforcing elements manufactured by three-dimensional printing; R = rounded reinforcing bar; ϕ = nominal diameter of strand. 1 mm = 0.0394 in.



Assembled state



Formwork with reinforcing elements

Figure 7. Formwork and reinforcement details.

Test setup and instrumentation

In pullout experiments of untensioned strands, hydraulic tensioning at the surface is generally used. This method has a problem: the compressive force, which acts as a reaction force of the tensioning force, applies pressure on the free end (upper surface), resulting in a stress distribution that differs from the condition where no reaction force is applied. To

accurately account for the effect of prestress, force must be transmitted solely through the bond stress of the strand to the concrete. Therefore, in this study, an actuator was used, instead of a hydraulic jack, to pull out the strand.

Figure 8 shows the test setup for the strand pullout experiment. The loading was applied using an actuator with a capacity of 500 kN (112.4 kip). The displacement measured

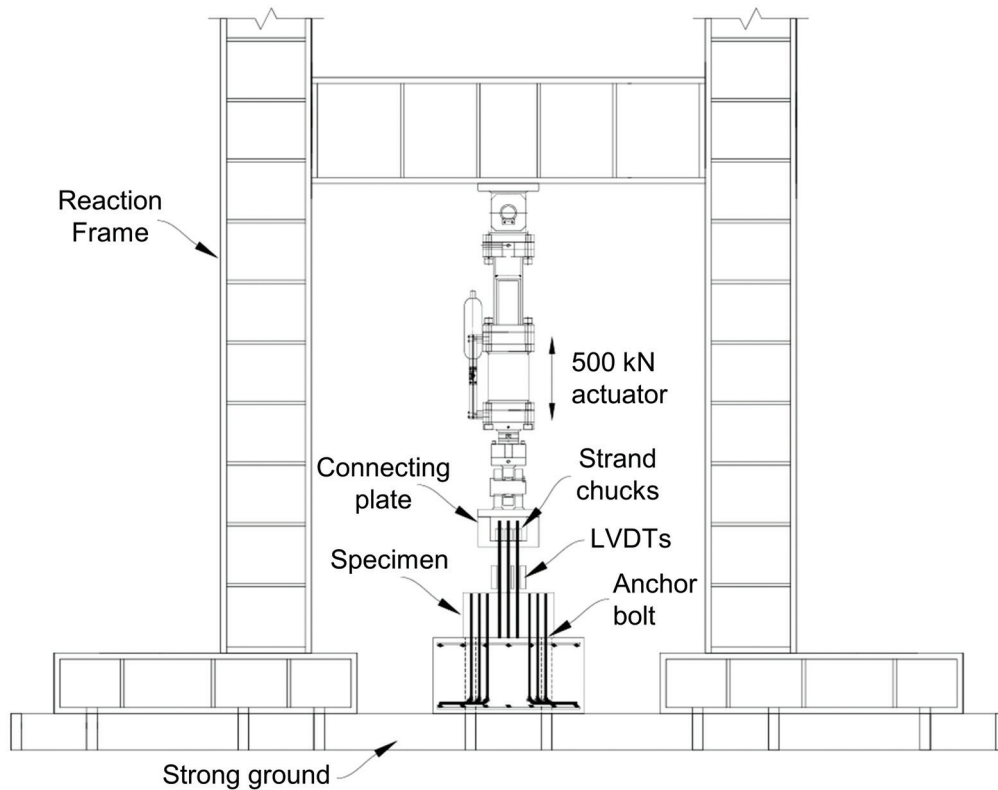


Figure 8. Test setup. Note: LVDT = linear variable displacement transducer. 1 kN = 0.225 kip.

by the linear variable differential transducers was used as the pullout displacement. Displacement control was adopted during the loading, and overall cracking patterns were recorded. To simultaneously pull out three strands embedded in each specimen, a connecting plate was fabricated and the strands were fixed on the top of the connecting plate using strand chucks.

Materials

Normalweight concrete with a 28-day design compressive strength f'_c of 30 MPa (4.4 ksi) was specified for all specimens. All cylinders were cast on the same day, along with casting specimens from each concrete truck, at a local concrete plant. Korean Standard (KS) SWPC7BL strands with a diameter of 12.7 mm (0.5 in.) and a tensile strength f_{pu} of 1860 MPa (270 ksi) were specified. The material properties of the 3-D-printed reinforcing elements were determined by submitting five specimens measuring 150 mm (5.85 in.) in length to direct tensile testing, and the material properties of metal lath were based on mill testing results. **Table 3** summarizes the material properties of the specimens.

Test results and observations

Observed crack patterns

During the strand pullout experiment, the amount of slip and the occurrence of cracks were monitored for each specimen.

Figure 9 presents the cracking patterns of the four specimens. It was observed that cracks first occurred at approximately 70% of the maximum pullout load in each specimen. The reentrant corner cracks originated from the free end and gradually extended to the opposite side as the displacement (slip) increased. In the PS-3DP-SOLID specimen, the spread of reentrant corner cracks could not be visually observed except from the top view because the reinforcing elements covered the surface.

Figure 10 shows the crack patterns observed on the upper surfaces. In the PS-NON, PS-3DP-HOLLOW, and PS-3DP-SOLID specimens, the shapes of the cracks observed in the connecting line between the strands and from the outermost strand to the concrete cover were consistent with the critical path defined by den Uijl.² In the PS-MESH specimen, cracks were observed around the embedding location of the reinforcing elements (metal lath) because the reinforcing elements were inside the concrete and not embedded on the concrete surface.

Tensile load-displacement relationship

Figures 11 and **12** present the tensile load-displacement relationship for each specimen, and **Table 4** summarizes the experimental results. In the PS-NON specimen, which did not have reentrant corner reinforcement, the tensile load increased as the displacement increased, and the specimen exhibited brittle behavior, in which the tensile load decreased after

Table 3. Material properties

Material	Item	Property
Strand (ϕ 12.7, SWPC7BL)	A_p , mm ²	98.7
	E_p , MPa	200,000*
	f_{py} , MPa	1580*
	f_{pu} , MPa	1860*
Concrete [†]	f'_c , MPa	33.7
	E_c , MPa	28,500*
3-D printed element [‡] (ABS-like resin)	f_y , MPa	62.8
	E , MPa	2650
Metal lath	f_y , MPa	170
	f_u , MPa	307
	E , MPa	20,000*

Note: 3-D = three-dimensional; ABS = acrylonitrile butadiene styrene; A_p = area of tension reinforcement; E = elastic modulus of material; E_c = elastic modulus of concrete; E_p = elastic modulus of tendon reinforcement; f'_c = compressive strength of concrete; f_{pu} = tensile strength of tendon reinforcement; f_{py} = yield strength of tendon reinforcement; f_u = tensile strength of material; f_y = yield strength of material; 3-D = three-dimensional; f = nominal diameter of strand. 1 mm = 0.0394 in.; 1 MPa = 0.145 ksi.

* Nominal values, not measured.

[†] Average based on three concrete cylinder specimens.

[‡] Average based on five specimens.



Figure 9. Crack patterns of each strand pullout experiment specimen. Note: PS-MESH = specimen with reentrant corners reinforced using metal lath; PS-NON = specimen with no reentrant corner crack reinforcing elements; PS-3DP-HOLLOW = specimen with hollow reinforcing elements manufactured by three-dimensional printing; PS-3DP-SOLID = specimen with solid reinforcing elements manufactured by three-dimensional printing.

reaching the maximum value. Compared with the PS-NON result, the maximum applied tensile load of PS-3DP-HOLLOW increased by 10.2%, the maximum applied tensile load of PS-3DP-SOLID increased by 8.0%, and the maximum applied tensile load of PS-MESH increased by 7.3%.

PS-3DP-HOLLOW exhibited the highest maximum applied tensile load, and even after reaching the maximum load, the load was higher than that of PS-NON. PS-3DP-SOLID showed higher maximum applied tensile load than PS-NON but exhibited almost the same behavior as PS-NON after reaching the maximum load. The superior performance of PS-3DP-HOLLOW was due to its ability to maintain adhesion

to the concrete after crack occurrence. Cracks originating from strand progressed toward the surface of the reinforcing elements, causing separation at the interface. With a hollow configuration, the interlocking effect occurred, which helped maintain some of the reinforcing effect. Because the PS-3DP-SOLID specimen was solid, adhesion was not maintained after crack occurrence, resulting in a loss of reinforcing effect. The reinforcing effect of mesh-type reinforcement is widely recognized, especially in textile-reinforced mortar methods¹⁸⁻²⁰ and in geotechnical applications, where mesh-type reinforcements such as geogrids exhibit better performance than geotextiles due to interlocking effects.²¹⁻²³ Although PS-3DP-SOLID had a larger amount of reinforcing elements than PS-



PS-NON



PS-3DP-HOLLOW



PS-3DP-SOLID



PS-MESH

Figure 10. Top view of crack patterns of each strand pullout experiment specimen. Note: PS-MESH = specimen with reentrant corners reinforced using metal lath; PS-NON = specimen with no reentrant corner crack reinforcing elements; PS-3DP-HOLLOW = specimen with hollow reinforcing elements manufactured by three-dimensional printing; PS-3DP-SOLID = specimen with solid reinforcing elements manufactured by three-dimensional printing.

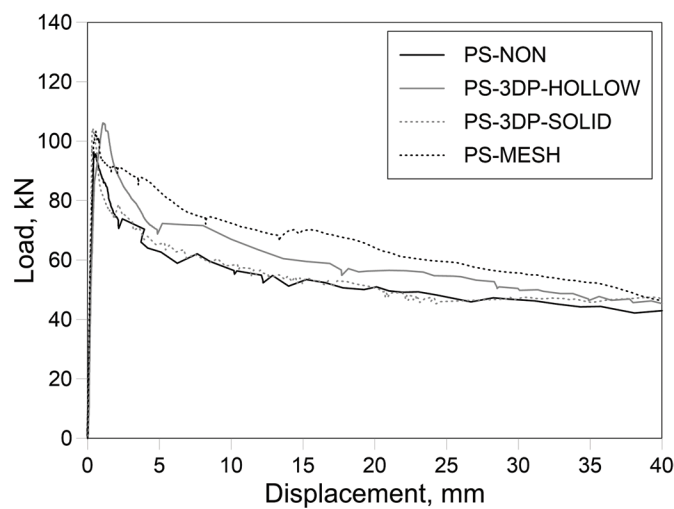


Figure 11. Load displacement relationship of strand pullout tests. Note: PS-MESH = specimen with reentrant corners reinforced using metal lath; PS-NON = specimen with no reentrant corner crack reinforcing elements; PS-3DP-HOLLOW = specimen with hollow reinforcing elements manufactured by three-dimensional printing; PS-3DP-SOLID = specimen with solid reinforcing elements manufactured by three-dimensional printing. 1 mm = 0.0394 in.; 1 kN = 0.225 kip.

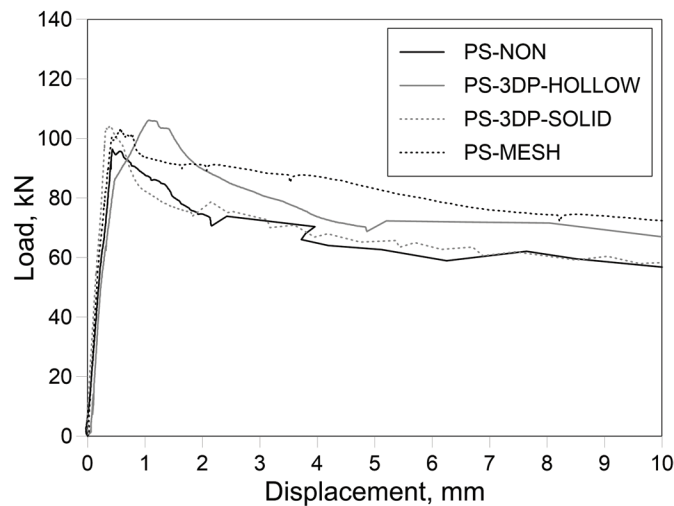


Figure 12. Load displacement relationship of strand pullout tests (up to 10 mm). Note: PS-MESH = specimen with reentrant corners reinforced using metal lath; PS-NON = specimen with no reentrant corner crack reinforcing elements; PS-3DP-HOLLOW = specimen with hollow reinforcing elements manufactured by three-dimensional printing; PS-3DP-SOLID = specimen with solid reinforcing elements manufactured by three-dimensional printing. 1 mm = 0.0394 in.; 1 kN = 0.225 kip.

Table 4. Summary of test results

Characteristics	PS-NON	PS-3DP-HOLLOW	PS-3DP-SOLID	PS-MESH
Maximum load, kN	96.3	106.1	104.0	103.3
Crack occurrence load, kN	75.0	78.0	n.d.*	72.0
Displacement at maximum load, mm	0.43	1.17	0.28	0.56

Note: n.d. = no data; PS-MESH = specimen with reentrant corners reinforced using metal lath; PS-NON = specimen with no reentrant corner crack reinforcing elements; PS-3DP-HOLLOW = specimen with hollow reinforcing elements manufactured by three-dimensional printing; PS-3DP-SOLID = specimen with solid reinforcing elements manufactured by three-dimensional printing. 1 mm = 0.0394 in.; 1 kN = 0.225 kip.

* This value was not visually observed because the surface was covered by the reinforcing element.

3DP-HOLLOW, the reinforcing effect in PS-3DP-SOLID was lower. This finding suggests that the formation of adhesion with concrete through internal hollows is more important than the strength of reinforcing elements.

PS-MESH exhibited ductile behavior, in which the tensile load gradually decreased as the displacement increased. When the displacement increased to 2 mm (0.079 in.), the tensile load decreased by only 11.8% compared with the maximum applied tensile load. Furthermore, even when the displacement increased to 5 mm (0.197 in.), the tensile load decreased by only 19.5% compared with the maximum applied tensile load. On the other hand, for PS-NON, when the displacement increased to 2 mm and 5 mm, the tensile load decreased by 22.6% and 34.9%, respectively.

There was a small difference in the peak load among all specimens, but a notable difference was observed in the post-peak behavior. This difference in post-peak behavior can be explained by the effect of reinforcement in preventing crack opening, based on the concrete confinement model.²⁴ That

model considers the concrete cylinder around the strands as a confining element against the expansion pressure caused by slip. The model exhibits three stages of behavior as cracks progress: the uncracked stage, the partially cracked stage, and the cracked stage. In the uncracked stage, no cracks occur in the concrete cylinder. In the partially cracked stage, cracks extend up to a certain length, at which point the confining stress reaches its maximum. In the cracked stage, cracks extend throughout the entire concrete cylinder. The maximum applied tensile load occurs in the partially cracked stage; however, since the reinforcement does not cross the crack surface at this stage, there is no significant difference in the confining capacity of a reinforced component and the confining capacity of a component without reinforcement. In the cracked stage, as the reinforcing elements prevent crack widening, the confining capacity reduction after the peak is smaller in specimens with reinforcement. This discussion is limited to the behavior of a section and does not consider the bond-slip behavior in the embedded length. Nonetheless, as the embedded length of the test specimen was as short as 300 mm (11.8 in.), the conclusions in this discussion remain

valid. This study, therefore, experimentally demonstrates that reinforcing elements placed across the reentrant corner cracks effectively prevent crack widening and help maintain the confining effect in pretensioned, prestressed components.

Analysis of the experimental results

Analysis model

In pretensioned, prestressed concrete components, the stress distribution around the strands can be expressed using the thick-walled cylinder model^{10,11} (Fig. 13), which considers the concrete around the strands as a hollow cylinder. During the strand pullout experiment, the stress of the strand increases, causing the expansion pressure $\sigma_{r,i}$ to act inside the concrete cylinder. The expansion pressure acting on the concrete cylinder and the confining stress acting on the strand have the same value.

During the pullout experiment, the expansion pressure inside the concrete cylinder is caused by the slip of the strand. The radial strain of a concrete cylinder can be determined from the value of slip and transfer length, and the expansion pressure is influenced by this radial strain.^{14,24–26} In this experiment, when the strand was tensioned, the diameter of the strand decreased due to Hoyer effect, but the expansion pressure occurred due to the effect of slip. The behavior differs from the push-in condition of pretensioned, prestressed concrete components; however, for comparing the pullout load when cracks occur, only the maximum expansion pressure (confining stress) and the friction coefficient are needed, and consideration of Hoyer effect is not necessary.

According to Tepfers,¹ the bond stress at the interface between the strand and concrete can be obtained by:

$$\tau_b = \tau_0 + \mu\sigma_{r,i}$$

where

τ_b = bond stress at the interface between the strand and concrete

τ_0 = bond stress due to the chemical adhesion

μ = friction coefficient

$\sigma_{r,i}$ = confining stress of concrete cylinder at inner radius

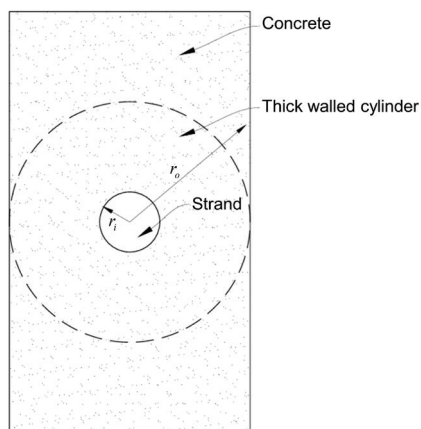
Assuming a rigid-brittle behavior of chemical adhesion,¹⁴ chemical adhesion can be regarded as 0 after initial slip occurs, and the bond stress at the interface between the strand and concrete can be expressed as τ_b equals $\mu\sigma_{r,i}$.

If the bond stress is obtained during the strand pullout experiment, the value of the confining stress $\sigma_{r,i}$ can be calculated by dividing the value of bond stress by the friction coefficient $\sigma_{r,i} = \tau_b/\mu$.

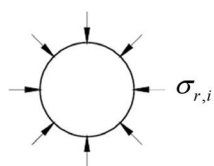
In the strand pullout experiment, the distribution of bond stress may have different values depending on the location. However, in this experiment, the length of the specimen is relatively short (300 mm [11.8 in.]), so it can be assumed that the bond stress is uniform over the entire length, and the average bond stress $\tau_{b,av}$ can be calculated as follows.

$$\tau_{b,av} = P_0/(\pi d_p L)$$

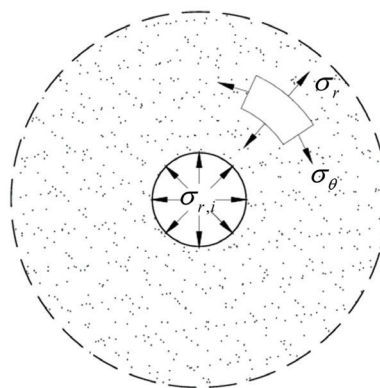
where



Thick-walled cylinder



Strand



Concrete cylinder

Figure 13. Thick-walled cylinder model. Note: r_i = inner radius of concrete cylinder; r_o = outer radius of concrete cylinder, σ_r = radial stress of concrete cylinder; $\sigma_{r,i}$ = confining stress of concrete cylinder at inner radius; σ_θ = circumferential stress of concrete cylinder.

- P_0 = pullout force
- d_p = strand diameter
- L = length of specimen

In the thick-walled cylinder model, the sum of expansion pressures caused by the strand and the sum of circumferential tensile stresses of the concrete cylinder must be balanced. The confining stress has a relationship with the tensile stress distribution in the circumferential direction of the concrete cylinder. To calculate the tensile stress distribution, the elastic model illustrated in **Fig. 14** can be applied.

The linear elastic behavior of a concrete cylinder before cracking was presented by Timoshenko¹³ as shown in the following equations.

$$\sigma_r(r) = \frac{r_i^2 p_i}{r_o^2 - r_i^2} \left(1 - \frac{r_o^2}{r^2} \right) = -p_i \times \frac{\frac{1}{r^2} - \frac{1}{r_o^2}}{\frac{1}{r_i^2} - \frac{1}{r_o^2}}$$

$$\sigma_\theta(r) = \frac{r_i^2 p_i}{r_o^2 - r_i^2} \left(1 + \frac{r_o^2}{r^2} \right) = p_i \times \frac{\frac{1}{r^2} + \frac{1}{r_o^2}}{\frac{1}{r_i^2} - \frac{1}{r_o^2}}$$

where

- σ_r = radial stress of concrete cylinder
- r = radius of concrete cylinder
- r_i = inner radius of concrete cylinder
- p_i = internal expansion pressure of concrete cylinder
- r_o = outer radius of concrete cylinder
- σ_θ = circumferential stress of concrete cylinder

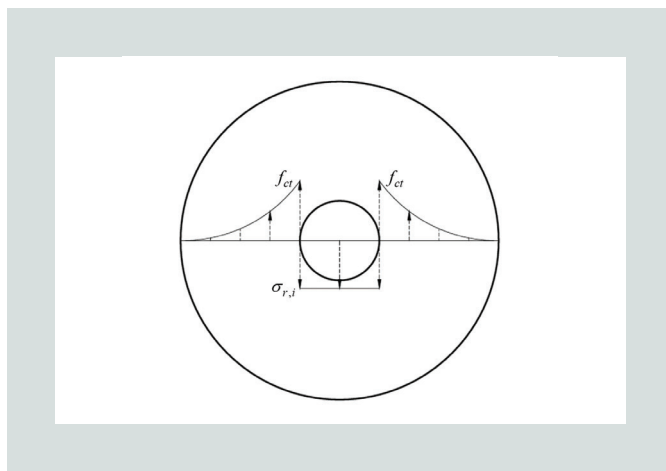


Figure 14. Stress distribution of the concrete cylinder elastic model. Note: f_{ct} = tensile strength of concrete; $\sigma_{r,i}$ = confining stress of concrete cylinder at inner radius.

The maximum circumferential tensile stress occurs at the interface between the strand and the concrete, and the maximum value of the circumferential stress in the concrete cylinder is same as the tensile strength of the concrete f_{ct} , as expressed in the following equation.

$$\sigma_\theta(r_i) = p_i \times \frac{\frac{1}{r_i^2} + \frac{1}{r_o^2}}{\frac{1}{r_i^2} - \frac{1}{r_o^2}} = f_{ct}$$

The following equation expresses the distribution of circumferential stress at the time of maximum stress.

$$\sigma_\theta(r) = p_i \times \frac{\frac{1}{r^2} + \frac{1}{r_o^2}}{\frac{1}{r_i^2} - \frac{1}{r_o^2}} = f_{ct} \times \frac{\frac{1}{r^2} + \frac{1}{r_o^2}}{\frac{1}{r_i^2} + \frac{1}{r_o^2}}$$

Therefore, the internal expansion pressure of a concrete cylinder $\sigma_{r,i}$ can be obtained by summing the tensile stresses over the entire thickness of the concrete cylinder and dividing the sum by the diameter of strand d_p .

$$\sigma_{r,i} = \frac{2}{d_p} \int_{r_i}^{r_o} \sigma_\theta(r) dr$$

Analysis results

The internal expansion pressures of concrete cylinder at crack occurrence from the results of PS-NON and PS-MESH were compared with the expansion pressure obtained from the elastic model. A typical friction coefficient value μ of 0.4 was used.^{27,28} In accordance with *fib* model code 2020,¹⁴ the following equations express the tensile strength of the concrete.

$$f_{ck} = f_{cm} = 33.7 \text{ MPa}$$

$$f_{ct} = 1.8 \ln(f_{ck}) - 3.1 = 3.23 \text{ MPa}$$

where

$$f_{ck} = \text{characteristic compressive strength of concrete}$$

$$f_{cm} = \text{mean compressive strength of concrete}$$

Since the thickness of the concrete cylinder is 38.1 mm (1.5 in.), the maximum internal expansion pressure has a value of 3.06 MPa (0.444 ksi) in the elastic model. By multiplying the maximum expansion pressure with the friction coefficient, the bond stress due to the elastic behavior of the concrete cylinder $\tau_{b,elastic}$ can be calculated.

$$\tau_{b,elastic} = 0.4 \times 3.06 = 1.22 \text{ MPa (0.177 ksi)}$$

The bond stresses of PS-NON and PS-MESH at crack occurrence, which are 2.09 MPa (3.03 ksi) and 2.00 MPa (0.290 ksi), respectively, are 71.3% and 63.9% higher than the bond stress due to elastic behavior $\tau_{b,elastic}$. Since the bond stress obtained by the elastic model represents a lower-limit

value, it was found the experimental values exceeded the lower limit when reentrant corner crack occurred.

Conclusion

Based on the results of this experimental investigation, the following conclusions are drawn:

- To investigate the reinforcing effect of pretensioned, prestressed concrete slabs on reentrant corner cracks, a pullout experiment was conducted by embedding untensioned strands in unit ribbed-shape specimens and then placing reinforcing elements around the strands. The results showed that the maximum applied tensile load increased as the confining effect of the concrete in reinforced specimens increased. In the two specimens with 3-D-printed reinforcing elements, PS-3DP-SOLID had a larger amount of reinforcement than PS-3DP-HOLLOW, but the maximum applied tensile load and ductility were greater in PS-3DP-HOLLOW due to the presence of hollows. It was found that an element with interior hollows was suitable for reentrant corner crack reinforcement. Specifically, the PS-MESH reinforced with metal lath exhibited a 7.8% increase in maximum applied tensile load and ductile behavior with tensile load decreasing only 11.8% even when displacement increased to 2 mm (0.0787 in.). Therefore, metal lath, which is made of ductile steel and has hollows inside, is beneficial as a reinforcing element for reentrant corner cracks.
- To confirm the confinement effect of a concrete cylinder when reentrant corner cracks occur, the bond stresses of PS-NON and PS-MESH were compared with the bond stress obtained by applying the elastic model to the concrete cylinder. The bond stress values of PS-NON and PS-MESH at the time of crack occurrence were 71.3% and 63.9% higher, respectively, than the predicted bond stress value of concrete cylinder. Although the measured bond stresses at the time of crack occurrence were higher than the predicted value, this study provides a useful reference for estimating the load at which reentrant crack occur.
- Reentrant corner cracks are common issues during the production process of pretensioned, prestressed concrete slabs, especially when the slabs are long and their cross sections are slender. In this experiment, the reinforced specimens were stronger and more ductile than the unreinforced specimen, which prevented crack widening. Based on the results of this experimental study, to reinforce the anticipated reentrant corner cracks in precast concrete slabs, it is effective to embed reinforcing elements with a right-angled shape and made of ductile materials.

Acknowledgments

The work presented was supported by the National Research Foundation of Korea (NRF-2021R1A5A1032433), CAMUS

E&C, and the Institute of Construction and Environmental Engineering at Seoul National University. The authors greatly appreciate the engineers of CAMUS E&C for their assistance.

References

1. Tepfers, R. 1973. "A Theory of Bond Applied to Overlapped Tensile Reinforcement Splices for Deformed Bars." PhD thesis, Chalmers University of Technology, Gothenburg Sweden.
2. den Uijl, J. A. 1983. *Tensile Stresses in the Transmission Zones of Hollow-core Slabs Prestressed with Pretensioned Strands*. Report 5-83-10. Delft, Netherlands: Stevin Laboratories, Delft University of Technology.
3. den Uijl, J. A. 1985. "Bond Properties of Strands in Connection with Transmission Zone Cracks." *Betonwerk und Fertigteil-Technik* 51 (1): 28–36.
4. Leskelä, M. V. 1990. "Push-out Test for Assessing the Bond Strength of Prestressing Tendons." *Nordic Concrete Research*, no. 9, 81–96.
5. ACI (American Concrete Institute). 2019. *Building Code Requirements for Concrete (ACI 318-19) and Commentary (ACI 318R-19)*. Farmington Hills, MI: ACI.
6. PCI. 2017. *PCI Design Handbook: Precast and Prestressed Concrete*. 8th ed. Chicago, IL: PCI.
7. fib (International Federation for Structural Concrete). 2007. *Treatment of Imperfections in Precast Structural Elements: State-of-the-Art Report*. Bulletin 41. Lausanne, Switzerland: fib.
8. PCI Committee on Quality Control Performance Criteria. 1983. "Fabrication and Shipment Cracks in Prestressed Hollow-core Slabs and Double Tees." *PCI Journal* 28 (1): 18–39. <https://doi.org/10.15554/pci28.1-03>.
9. Raja, S. R. 2018. "Stresses in the End Zones of Precast Inverted T-Beams with Tapered Webs." MS thesis, Wayne State University, Detroit, MI.
10. Timoshenko, S. 1976. *Strength of Materials. Part II. Advanced Theory and Problems*. 3rd ed. New York, NY: Van Nostrand Reinhold.
11. Ugural, A. C., and S. K. Fenster. 2012. *Advanced Mechanics of Materials and Applied Elasticity*. 5th ed. New York, NY: Pearson Education.
12. Coccia, S., E. di Maggio, and Z. Rinaldi. 2015. "Bond Slip Model in Cylindrical Reinforced Concrete Elements Confined with Stirrups." *International Journal of*

Advanced Structural Engineering, no. 7, 365–375.
<https://doi.org/10.1007/s40091-015-0104-7>.

13. fib. 2013. *fib Model Code for Concrete Structures (2010)*. Lausanne, Switzerland: fib.
14. fib. 2023. *fib Model Code for Concrete Structures (2020)*. Lausanne, Switzerland: fib.
15. Russell, B. W., and N. H. Burns. 1993. *Design Guidelines for Transfer, Development and Debonding of Large Diameter Seven Wire Strands in Pretensioned Concrete Girders*. FHWA/TX-93+1210-5F. Austin, TX: Center for Transportation Research, University of Texas at Austin. <https://library.ctr.utexas.edu/digitized/texasarchive/phase2/1210-5f.pdf>.
16. Barnes, R. W., N. H. Burns, and M. E. Kreger. 1999. *Development Length of 0.6-Inch Prestressing Strand in Standard I-shaped Pretensioned Concrete Beams*. FHWA/TX-02/1388-1. Austin, TX: Center for Transportation Research, University of Texas at Austin. <https://library.ctr.utexas.edu/ctr-publications/1388-1.pdf>.
17. AASHTO (American Association of State Highway and Transportation Officials). 2020. *AASHTO LRFDP Bridge Design Specifications*. 9th ed. Washington, DC: AASHTO.
18. Papanicolaou, C. G., T. C. Triantafyllou, K. Karlos, and M. Papathanasiou. 2007. “Textile-Reinforced Mortar (TRM) versus FRP as Strengthening Material of URM Walls: In-Plane Cyclic Loading.” *Materials and Structures*, no. 40, 1081–1097. <https://doi.org/10.1617/s11527-006-9207-8>.
19. Torres, B., S. Ivorra, F. J. Baeza, L. Estevan, and B. Varona. 2021. “Textile Reinforced Mortars (TRM) for Repairing and Retrofitting Masonry Walls Subjected to In-Plane Cyclic Loads. An Experimental Approach.” *Engineering Structures*, no. 231, 111742. <https://doi.org/10.1016/j.engstruct.2020.111742>.
20. Padalu, P. K. V. R., S. Trivedi, S. Gaulkar, R. Vashisht, and V. Kumar. 2024. “Seismic Retrofitting Systems for Unreinforced Masonry from a Rural Community Perspective: An Overview.” *Iranian Journal of Science and Technology, Transactions of Civil Engineering*, 1–71. <https://doi.org/10.1007/s40996-024-01654-9>.
21. Zhang, J., and G. Hurta. 2008. “Comparison of Geotextile and Geogrid Reinforcement on Unpaved Road.” In *GeoCongress 2008: Geosustainability and Geohazard Mitigation*, pp. 530–537. Reston, VA: ASCE (American Society of Civil Engineers). [https://doi.org/10.1061/40971\(310\)66](https://doi.org/10.1061/40971(310)66).
22. Nan-Liu, C., J. G. Zornberg, T. C. Chen, Y. H. Ho, and B. H. Lin. 2009. “Behavior of Geogrid-Sand Interface in Direct Shear Mode.” *Journal of Geotechnical and Geoenvironmental Engineering* 135 (12): 1863–1871. [https://doi.org/10.1061/\(ASCE\)GT.1943-5606.0000150](https://doi.org/10.1061/(ASCE)GT.1943-5606.0000150).
23. Choudhary, A. K., and A. M. Krishna. 2016. “Experimental Investigation of Interface Behaviour of Different Types of Granular Soil/Geosynthetics.” *International Journal of Geosynthetics and Ground Engineering*, no. 2, 4. <https://doi.org/10.1007/s40891-016-0044-8>.
24. den Uijl, J. A., and A. J. Bigaj. 1996. “A Bond Model for Ribbed Bars on Concrete Confinement.” *HERON* 41 (3): 201–226. <https://heronjournal.nl/41-3/4.pdf>.
25. den Uijl, J. A. 1998. “Bond Modelling of Prestressing Strand.” *ACI Special Publication*, no. 180, 145–169. <https://doi.org/10.14359/5876>.
26. Steensels, R., L. Vandewalle, B. Vandoren, and H. Degée. 2017. “A Two-Stage Modelling Approach for the Analysis of the Stress Distribution in Anchorage Zones of Pre-Tensioned, Concrete Elements.” *Engineering Structures*, no. 143, 384–397. <https://doi.org/10.1016/j.engstruct.2017.04.011>.
27. Tepfers, R. 1979. “Cracking of Concrete Cover Along Anchored Deformed Reinforcing Bars.” *Magazine of Concrete Research* 31 (106): 3–12. <https://doi.org/10.1680/mac.1979.31.106.3>.
28. Janney, J. R. 1954. “Nature of Bond in Pretensioned Prestressed Concrete.” *ACI Journal* 50 (5): 717–736. <https://doi.org/10.14359/11790>.

Notation

A_p	= area of tension reinforcement
d	= distance from compressive face to centroid of tension reinforcement
d_p	= strand diameter
E	= elastic modulus of material
E_c	= elastic modulus of concrete
E_p	= elastic modulus of tendon reinforcement
f'_c	= compressive strength of concrete
f_{ck}	= characteristic compressive strength of concrete
f_{cm}	= mean compressive strength of concrete
f_{ct}	= tensile strength of concrete

f_{pu}	= tensile strength of tendon reinforcement
f_{py}	= yield strength of tendon reinforcement
f_u	= tensile strength of material
f_y	= yield strength of material
L	= length of specimen
P_0	= pullout force
p_i	= internal expansion pressure of concrete cylinder
r	= radius of concrete cylinder
r_i	= inner radius of concrete cylinder
r_o	= outer radius of concrete cylinder
t	= thickness of strand
T	= initial prestress
w	= width of strand
ΔT	= increased prestress due to bond behavior
μ	= friction coefficient
σ_r	= radial stress of concrete cylinder
$\sigma_{r,i}$	= confining stress of concrete cylinder at inner radius
σ_θ	= circumferential stress of concrete cylinder
τ_0	= bond stress due to chemical adhesion
τ_b	= bond stress at the interface between strand and concrete
$\tau_{b,av}$	= average bond stress at the interface between strand and concrete
$\tau_{b,elastic}$	= bond stress due to elastic behavior of concrete cylinder at the interface
ϕ	= nominal diameter of strand



Manwoo Kim is a PhD student in the Department of Architecture and Architectural Engineering at Seoul National University, Seoul, Korea.



Thomas H.-K. Kang, PhD, PE, is a professor in the Department of Architecture and Architectural Engineering at Seoul National University.

Abstract

Reentrant corner cracks have been observed in pre-tensioned concrete slabs, but the phenomenon has not been explained in relation to the introduction of prestressing. In this study, a strand pullout experiment was conducted to confirm the occurrence of reentrant corner cracks and investigate the effect of reinforcement on these cracks. The specimens were made in the shape of a unit rib of an inverted ribbed precast concrete slab, and three types of reinforcing elements were placed across the predicted surfaces of the cracks. The results showed that the maximum applied tensile load increased by up to 10.2% with reinforcement. In the specimen with mesh reinforcement, when the slip increased to 2 mm (0.079 in.), the load reduction ratio was limited to 52.2% of that of the unreinforced specimen. These findings provide practical insights into the behavior of reentrant corner cracks, enhancing understanding of how reinforcement can effectively maintain structural integrity.

Keywords

Confining effect, crack prevention, pullout experiment, reentrant corner, thick-walled cylinder model.

Review policy

This paper was reviewed in accordance with the Precast/Prestressed Concrete Institute's peer-review process. The Precast/Prestressed Concrete Institute is not responsible for statements made by authors of papers in *PCI Journal*. No payment is offered.

Publishing details

This paper appears in *PCI Journal* (ISSN 0887-9672) V. 70, No. 3, May–June 2025, and can be found at <https://doi.org/10.15554/pcij70.3-02>. *PCI Journal* is published bimonthly by the Precast/Prestressed Concrete Institute, 8770 W. Bryn Mawr Ave., Suite 1150, Chicago, IL 60631. Copyright © 2025, Precast/Prestressed Concrete Institute.

Reader comments

Please address any reader comments to *PCI Journal* editor-in-chief Tom Klemens at tklemens@pci.org or Precast/Prestressed Concrete Institute, c/o *PCI Journal*, 8770 W. Bryn Mawr Ave., Suite 1150, Chicago, IL 60631.